Article

Economic and Low-Carbon-Oriented Distribution Network Planning Considering the Uncertainties of Photovoltaic Generation and Load Demand to Achieve Their Reliability

Weifeng Xu [1], Bing Yu [1], Qing Song [1], Liguo Weng [1], Man Luo [1] and Fan Zhang [2],*

[1] State Grid Hangzhou Xiaoshan Power Supply Company, Hangzhou 311200, China
[2] College of Automation, Hangzhou Dianzi University, Hangzhou 310018, China
* Correspondence: zhangfan@hdu.edu.cn

Abstract: The integration of renewable resources with distribution networks (DNs) is an effective way to reduce carbon emissions in energy systems. In this paper, an economic and low-carbon-oriented optimal planning solution for the integration of photovoltaic generation (PV) and an energy storage system (ESS) in DNs is proposed. A convolutional neural network (CNN)-based prediction model is adopted to characterize the uncertainties of PV and load demand in advance. Then, taking the lowest total economic cost, the largest carbon emission reduction, and the highest system power supply reliability as the optimization objectives, the optimal distribution network planning model is constructed. The improved multi-objective particle swarm optimization (MOPSO) algorithm is used to solve the optimization model, and the effectiveness of the proposed solution is confirmed through a comparative case study on the IEEE-33 bus system. Simulation results show that the proposed solution can better maintain the balance between economic cost and carbon emissions in DNs.

Keywords: carbon emission; photovoltaic generation; energy storage system; distribution network planning; uncertainty modeling

1. Introduction

With the intensification of the greenhouse effect and the global energy supply problem, building a new low-carbon power system has become a consensus [1]. With the integration of distributed generation (DG), the traditional distribution networks are facing many new challenges [2], e.g., the output curves of PV and load are difficult to match to each other, which leads to increased network loss, decreased power supply quality, and reduced stability of the DNs [3]. As a key technology of the DNs, the energy storage system has the advantages of fast power response, high adjustment accuracy, and flexible configuration location [4], which can effectively mitigate the impact of PV output fluctuations on the DNs, maintain the frequency stability, and improve the power supply quality. The access of PV and ESS has greatly changed the structure and operation state of traditional DNs [5]; therefore, in order to improve the comprehensive benefits of the power system, the optimal location and capacity configuration of PV and ESS have become two of the focuses in this research area [6].

Uncertainty modeling in source-side and load-side is the basis of distribution network planning [7]. In [8], a short-term PV power prediction method combining improved *K*-means clustering, grey relational analysis (GRA), and an Elman neural network was proposed. The work in [9] constructed a hybrid short-term PV generation forecasting model in microgrid; a particle swarm optimization (PSO) and support vector machine (SVM) were adopted in this solution. In [10], a probabilistic prediction model based on a CNN for regional PV generation was presented. In [11], a hybrid machine learning-based algorithm was proposed for short-term wind power forecasting. As for load forecasting, reference [12] proposed a short-term load forecasting model which fully considered solar

radiation and historical electricity consumption data. In [13], a weighted hybrid support vector regression (SVR) method was adopted to predict the electricity demand in buildings. In [14], a load prediction model for electric market participants was proposed. In [15], a long short-term memory (LSTM)-based short-term load prediction method that considered residential characteristics was formulated.

In addition, much effort has been made in distribution network optimal planning issues. In [16], the capacities of various ESS in a microgrid system were optimized while also considering the power supply and demand characteristics. In [17], the location and sizing of hydrogen systems was solved to improve the performances of DNs. A combined framework for distribution network expansion planning and an energy storage system configuration in an active distribution network (ADN) was proposed in reference [18] to minimize the investment and grid loss. The study in [19] carried out an optimal allocation method for DNs with different combinations of PV-DGs, gas turbine-based DGs, and distribution static compensators. The study in [20] proposed an optimal configuration and operation solution of DG and ESS in which the energy dispatch problem was considered simultaneously. In addition, in [21], a water cycle algorithm (WCA) was adopted to solve the optimal planning model for DGs in an ADN. In [22], an optimal planning model for DGs in a passive distribution network (PDN) was proposed, and the load scenarios were incorporated into the model. In [23], an optimal capacity configuration solution for wind, PV, and ESS in DNs was formulated, and flicker emission was considered to improve the DN's performance. However, the aforementioned work did not take carbon emissions and the uncertainties of DGs into consideration.

In summary, there still remain several technical problems in distribution network planning that need further investigation: the uncertainties of PV and load have not been fully considered. Most of the existing research only uses historical data on typical days in the planning process. In addition, carbon emissions are rarely considered in distribution network planning. Most of the existing research only focuses on economic factors and system reliability. Finally, the number of studies which incorporate the uncertainty modeling and carbon emission analysis into distribution network planning is relatively few, and the existing research still needs to be further improved.

To this end, this paper proposes an optimal location and capacity allocation method of PV and energy storage in distribution networks that considers multiple uncertainties and system carbon emissions. The overall structure of the proposed solution is shown in Figure 1. Compared with the aforementioned research, the main contributions of this work can be summarized as follows. Firstly, a CNN-based scenario generation model is adopted to characterize the uncertainties of PV and load. Secondly, an optimal location and capacity configuration model for PV and ESS in DNs is proposed, and, taking the lowest total system cost, the largest carbon emission reduction, and the highest system power supply reliability as the objective functions, a new solution for distribution network planning is formulated. Finally, an improved MOPSO algorithm is used to solve the planning model, which has a faster convergence speed and a better quality optimal solution.

The rest of the paper is organized as follows. In Section 2, a CNN-based prediction model is constructed to characterize the multiple uncertainties. Section 3 proposes an optimal location and capacity configuration model of PV and batteries in a distribution network. Section 4 adopts an improved MOPSO algorithm to solve the optimization model. In Section 5, the proposed solution is assessed through a comparative study on the IEEE-33 bus system, and finally, the conclusive remarks are given in Section 6.
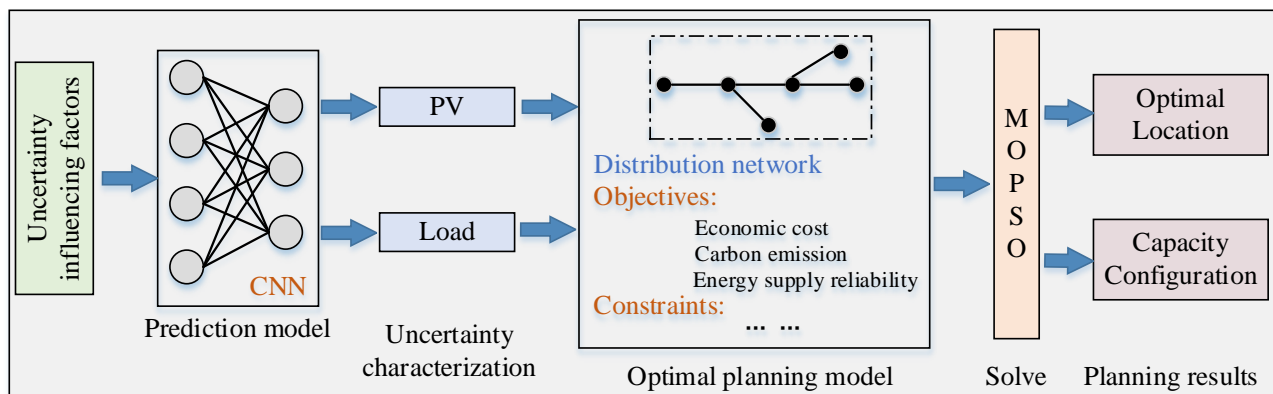
**Figure 1.** The overview of the proposed planning solution in DNs.

2. Uncertainty Characterization of PV and Load

Distributed power generation mainly contains PV generation and wind power generation. Compared with traditional generation methods, DG has the advantages of low carbon emissions and high economic benefits. However, the output of DG is affected by weather conditions, environmental temperature, wind speed, solar intensity, seasonal characteristics, and other factors, which results in strong randomness and volatility. Driven by the development of technologies, a large number of distributed power sources have been connected to the DNs, and the active distribution network is constructed. The main problems in the ADN during the operation process can be summarized as follows: firstly, the massive installed capacity of DG in the DNs leads to power reversal; secondly, affected by weather conditions, the local load cannot be fully met when the power generation of DG is reduced. Therefore, the energy storage system should be added to the DNs, which can suppress the power fluctuation caused by the randomness of DG, as well as improve the consumption rate of renewable energy effectively.

In order to ensure the operational stability of the DNs, a CNN-based method is adopted to model the uncertainties of PV and load in the distribution networks.

2.1. Basic CNN Model

CNN is a feed-forward neural network with deep convolutional structures. The topology of a typical CNN is shown in Figure 2. The fundamental structure mainly includes an input layer, output layer, convolutional layer, pooling layer, and fully connected layer [24]. The function of the convolutional layer is feature extraction, and the characteristics and distributions of input data are extracted by a convolution calculation. The pooling layer is generally located behind the convolutional layer and its role is to reduce the size of neurons in the convolutional layer using a down-sampling method. The fully connected layer is generally located in front of the output layer, which is mainly used to integrate the features extracted by the CNN, and to perform regression analyses based on them.
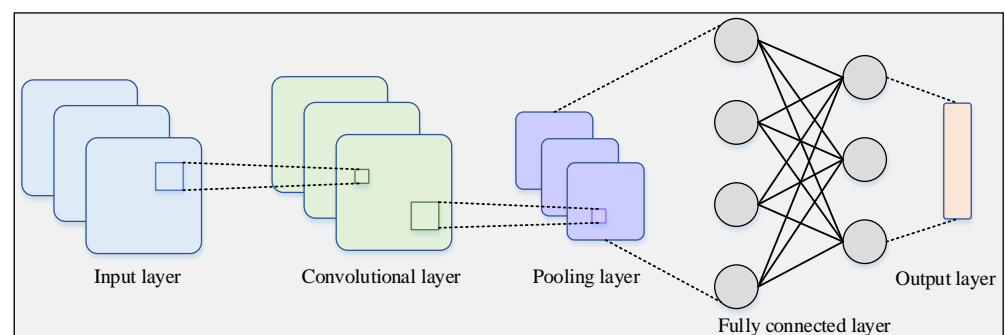
Figure 2. The structure diagram of a typical CNN.

The CNN in this study is trained using the gradient descent method, which searches for the optimal solution along the negative gradient direction of the parameters during the iteration process. The update formula is shown in (1):

$$\begin{cases} \delta w(t) = \left. \frac{\partial f_{obj}}{\partial w} \right|_{w=w(t)} \\ w(t+1) = w(t) - D_t \delta w(t) \end{cases} \tag{1}$$

where ω denotes the set of parameters in the CNN (weight and bias of convolution kernel and full connected layer), t denotes the number of iterations, f_{obj} denotes the target function of training, $\delta \omega(t)$ denotes the gradient of ω, and D_t denotes the step size of iteration.

In this study, the cross-entropy loss function is used to construct the training objective function of the CNN. The cross-entropy loss function is shown in (2):

$$Loss_{entropy} = -\frac{1}{n} \sum_x [y \ln(a) + (1-y) \ln(1-a)] \tag{2}$$

where x denotes the input of the CNN, and a and y denote the real output and expected output of the CNN.

For a training sample set: $\{Q_i = (\overline{x}_i, \overline{y}_i)\}_{i=1}^{N}$, $\overline{y}_i = (y_i^1, y_i^2 \dots y_i^R)$, the training objective function of the CNN model based on the cross-entropy loss function is shown in (3):

$$\min_w -\frac{1}{N} \sum_{i=1}^{N} \sum_{j=1}^{R} [y_i^j \ln(a_i^j) + (1-y_i^j) \ln(1-a_i^j)] \tag{3}$$

where N denotes the total number of samples, R denotes the amount of data contained in each output, and a_i^j and y_i^j represent the actual value and expected value of the jth data in the ith output group of the model.

2.2. CNN-Based Uncertainty Characterization Model for PV and Load

The solar radiation intensity will change due to different seasons and times, and therefore PV shows the characteristics of periodic changes. In addition, there are many other factors that will affect the output power of PV, including environmental temperature, environmental humidity, atmospheric pressure, and the parameters of photovoltaic panels. As an important part of the DN system, load is mainly affected by the price of electricity, temperature, humidity, historical load value, date, economic development level, and other factors. The characteristic information of the load is included in these data. If all influencing factors are used as the input of the uncertainty characterization model, it will lead to feature redundancy, increase the complexity of the prediction model, and affect the accuracy of the scenarios. Therefore, the influence factor screening method based on the correlation coefficient proposed in [8] is adopted in this paper. For the uncertainty characterization of PV generation, solar radiation intensity, ambient temperature, and ambient humidity are selected as the input; for the load uncertainty characterization, historical load value and electricity price are selected as the input.

The relationship between real PV and real load is influenced by many factors, e.g., the dynamic and time-varying nature of weather in the local area, the nonlinear and bounded power conversion process, and the complex spatial and temporal interactions, which are hard to simplify. Thus, a CNN-based method is used in this work. As a data-driven approach, this method does not need to assume that the historical data obey certain probability distributions in advance, it can spontaneously learn the implicit relationship between real PV and real load and generate PV and load scenarios with accuracy.

The uncertainty characterization model based on the CNN constructed in this paper is shown in Figure 3. The input of the model is the influencing factors. The input layer transmits data to the convolutional layer, which uses multiple convolutional kernels to extract the deep nonlinear characteristics between the influencing factors and PV and

load power, then the activation function is used to filter the extracted features. Finally, regression analysis is conducted on the filtered features through the fully connected layer to obtain the mapping relationship between the PV generation characteristics and the corresponding load characteristics and environmental factors. The input data (historical data) and output data (learning target) of the training model can be composed of the data from other distribution network data in the adjacent area. The well-trained CNN can use the existing meteorological and load data to predict the corresponding photovoltaic output characteristics, so as to obtain the photovoltaic power generation curve associated with the uncertainty of the local load and form a set of source–load coupling operation scenarios for optimizing the capacities of PV and energy storage.
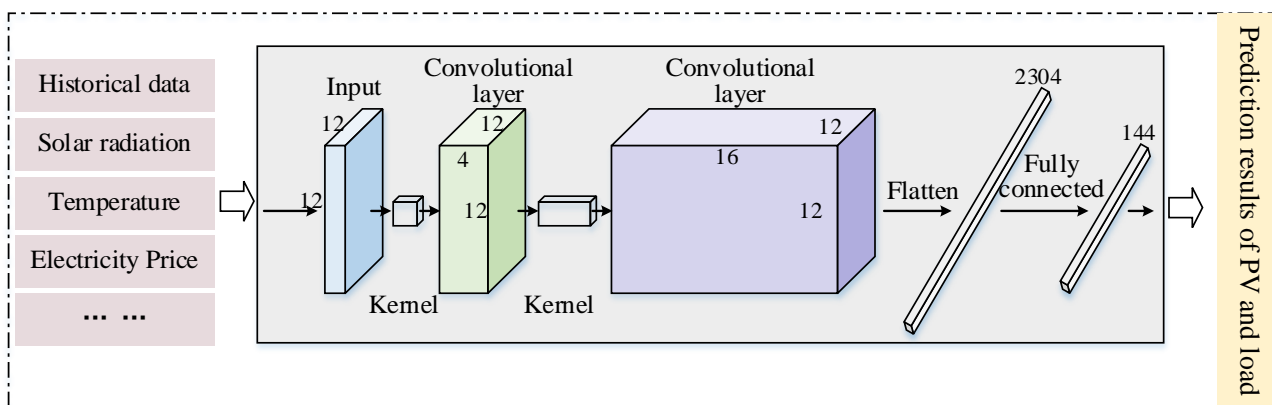

Figure 3. CNN-based prediction model for PV generation and load.

3. Optimal Location and Capacity Configuration Model for PV and ESS in DNs

To improve the carbon emission reduction capacity of the DNs, an optimal planning model for the location and capacity configuration of PV and energy storage in the DNs is constructed which fully considers the uncertainties of PV and load demand. This model can reduce the investment cost of PV and energy storage equipment, reduce the carbon emissions of the DNs, improve the utilization rate of PV, stabilize the power fluctuation, and improve the energy supply quality.

3.1. Objectives

Combined with the prediction results, the objective functions of this optimization model mainly include three indicators: system economic cost; system carbon emission reduction; and system power supply reliability.

3.1.1. Economic Cost

The life cycle of PV and batteries in the DNs mainly includes three stages: construction; operation and maintenance; and recycling. In the distribution network planning, the first two points need to be fully considered:

$$\min \text{Cost}_{sum} = C_{investment} + C_{opera-main} + C_{grid-buy} + C_{line} \tag{4}$$

where Cost_{sum}, $C_{investment}$, $C_{opera-main}$, $C_{grid-buy}$ and C_{line} denote the total economic cost, investment cost, operation and maintenance cost, power purchase cost from the main grid, and transmission line construction cost of the system, respectively.

$$C_{investment} = \frac{\varsigma(1+\varsigma)^n}{(1+\varsigma)^n - 1} \cdot \left(c_{invest}^{PV} \sum_{j=1}^{N} \lambda_j^{PV} P_j^{PV} + c_{invest}^{ESS} \sum_{j=1}^{N} \lambda_j^{ESS} P_j^{ESS} \right) \tag{5}$$

where n represents the total planning years, N is the total number of nodes in the distribution network, ς represents the discount rate, c_{invest}^{PV} and c_{invest}^{ESS} represent the unit investment

cost of PV and energy storage (0–1 variable), λ_j^{PV} and λ_j^{ESS} represent whether PV and energy storage are connected at node j, and P_j^{PV} and P_j^{ESS} represent the actual access capacities of PV and energy storage at node j.

$$C_{opera-main} = \frac{\varsigma(1+\varsigma)^n}{(1+\varsigma)^n - 1} \cdot \left(c_{opera-main}^{PV} \sum_{j=1}^{N} n\lambda_j^{PV} P_j^{PV} + c_{opera-main}^{ESS} \sum_{j=1}^{N} n\lambda_j^{ESS} P_j^{ESS} \right) \quad (6)$$

where $c_{opera-main}^{PV}$ and $c_{opera-main}^{ESS}$ denote the unit annual operation and maintenance costs of PV and energy storage, respectively.

$$C_{grid-buy} = c_{grid}(t) \cdot \sum_{i=1}^{n} \sum_{t=1}^{8760} \sum_{j=1}^{N} [P_{i,j}^{Load}(t) - P_{i,j}^{PV}(t) - P_{i,j}^{ESS\_dis}(t) + P_{i,j}^{ESS\_char}(t)] \quad (7)$$

where $c_{grid}(t)$ refers to the real-time electricity price from the grid at time t, $P_{i,j}^{Load}(t)$ and $P_{i,j}^{PV}(t)$ refer to the load power and PV power at the node j at time t of the ith year, and $P_{i,j}^{ESS\_char}(t)$ and $P_{i,j}^{ESS\_dis}(t)$ refer to the charging and discharge power of the ESS.

$$C_{line} = \frac{\varsigma(1+\varsigma)^n}{(1+\varsigma)^n - 1} \cdot \left(c_{construct}^{line} \cdot d_{line} \right) \quad (8)$$

where $c_{construct}^{line}$ denotes the unit investment cost of transmission lines and d_{line} denotes the total length of transmission lines to be constructed.

3.1.2. Carbon Emission Reduction

Carbon emission reduction represents the difference of carbon emissions between the original distribution network and the improved distribution network with PV generation and ESS.

$$\max C_{CO2}^{reduc} = \tau_{CO2} \cdot \sum_{i=1}^{n} \sum_{t=1}^{8760} \sum_{j=1}^{N} \left| \frac{C_{grid-buy}}{c_{grid}(t)} - P_{i,j}^{Load}(t) \right| \quad (9)$$

where C_{CO2}^{reduc} represents the total carbon emission reduction of the DNs in the planning period, τ_{CO2} represents the carbon emission coefficient of the thermal power generation, and $P_{i,j}^{Load}(t)$ represents the load power at node j at time t of the ith year.

3.1.3. Power Supply Reliability

For a typical distribution network, it is crucial to meet the load demand. Thus, the power supply reliability objective function is shown as follows:

$$\max C_{reliable} = \frac{1}{8760 \cdot nN} \cdot \sum_{i=1}^{n} \sum_{t=1}^{8760} \sum_{j=1}^{N} \frac{P_{i,j}^{PV}(t)}{P_{i,j}^{Load}(t) - P_{i,j}^{grid-buy}(t)} \quad (10)$$

where $C_{reliable}$ represents the power supply reliability of the DNs, and $P_{i,j}^{Load}(t)$, $P_{i,j}^{PV}(t)$ and $P_{i,j}^{grid-buy}(t)$ represent the load power, PV power, and purchasing power at node j at time t of the ith year.

3.2. Constraints

In the optimization model of the distribution network system considering the source- and load-side uncertainties proposed in this paper, power flow constraints, investment constraints, and operation constraints of PV and ESS are the main constraints to be considered.

3.2.1. Power Flow Constraints

The power flow constraints of the distribution network are shown as follows:

$$
\begin{cases}
P_i(t) = U_i(t) \sum_{j=1}^{N} U_j(t) \cdot [B_{ij}(t) \sin \theta_{ij}(t) + G_{ij}(t) \cos \theta_{ij}(t)] \\
Q_i(t) = U_i(t) \sum_{j=1}^{N} U_j(t) \cdot [G_{ij}(t) \sin \theta_{ij}(t) - B_{ij}(t) \cos \theta_{ij}(t)]
\end{cases}
\tag{11}
$$

where $P_i(t)$ and $Q_i(t)$ represent the active power and reactive power of the node i at time t, $U_i(t)$ and $U_j(t)$ represent the voltage of node i and node j at time t, respectively, $G_{ij}(t)$ and $B_{ij}(t)$ represent the susceptance and conductivity between node i and j at time t, respectively, and $\theta_{ij}(t)$ represents the voltage phase angle between node i and j at time t.

3.2.2. Investment Constraints

The maximum investment cost constraints of the distribution network are shown as follows:

$$
c_{invest}^{PV} \cdot \frac{\varsigma(1+\varsigma)^n}{(1+\varsigma)^n - 1} \cdot \sum_{j=1}^{N} \lambda_j^{PV} P_j^{PV} \leq C_{invest\_max}^{PV}
\tag{12}
$$

$$
c_{invest}^{ESS} \cdot \frac{\varsigma(1+\varsigma)^n}{(1+\varsigma)^n - 1} \cdot \sum_{j=1}^{N} \lambda_j^{ESS} P_j^{ESS} \leq C_{invest\_max}^{ESS}
\tag{13}
$$

where $C_{invest\_max}^{PV}$ and $C_{invest\_max}^{ESS}$ represent the maximum investment limit of PV and ESS in DNs, respectively.

3.2.3. Operation Constraints of PV

The operation constraint of PV in the distribution network is shown as follows:

$$
0 \leq P_j^{PV}(t) \leq P^{PV\_max}
\tag{14}
$$

where P^{PV_max} represents the maximum output power limit of PV generation.

3.2.4. Operation Constraints of ESS

The operation constraints of energy storage in the distribution network are shown as follows:

$$
\Psi^{ESS\_min} \leq \Psi_j^{ESS} \leq \Psi^{ESS\_max}
\tag{15}
$$

$$
P^{ESS\_min} \leq P_j^{ESS}(t) \leq P^{ESS\_max}
\tag{16}
$$

$$
SOC^{ESS\_min} \leq SOC_j^{ESS}(t) \leq SOC^{ESS\_max}
\tag{17}
$$

where Ψ^{ESS_max} and Ψ^{ESS_min} represent the upper and lower limits of the capacity of the ESS, P^{ESS_max} and P^{ESS_min} represent the upper and lower limits of the charging and discharging power of the ESS, and SOC^{ESS_max} and SOC^{ESS_min} represent the upper and lower limits of the state of charge of the ESS.

4. Improved Model-Solving Algorithm

Compared with single objective optimization problems, multi-objective optimization problems generally cannot give a specific solution that satisfies the optimization of all objective functions. Compromises must be made to make the overall objective function optimal, so as to obtain multiple groups of parallel solutions, which are presented in the form of Pareto solution sets. The optimal planning model proposed in this paper contains three different objective functions; therefore, an improved multi-objective particle swarm optimization algorithm is used to solve the model to find the best location and capacities of PV and ESS. The location information carried by each particle is an optional scheme,

which is constantly updated in the search space until a group of appropriate global optimal solutions is found.

However, the traditional MOPSO algorithm can have many defects when dealing with high-dimensional problems, such as the problem of too-fast particle aggregation, which leads to the lack of diversity of the particle population. Therefore, this paper introduces a quasi-opposition-based learning (QOBL) strategy in the generation and update process of the particles. A mixed population is formed by incorporating the obtained quasi-opposite population into the initial population, and then the first half of the individuals with high fitness is selected and inputted into the next iteration according to the dominance relationship and crowding distance of particles. The improved algorithm has simple parameter settings, a faster convergence speed, and a higher solution quality. The basic steps of the improved algorithm are as follows:

- Step 1. Input the related data of the distribution network and CNN-based prediction results;
- Step 2. Set the parameters of the MOPSO algorithm, including learning factors c_1 and c_2, weight coefficient w, population size N, maximum number of iterations K, and upper limit of particle flight speed $v_{\max}$, etc;
- Step 3. Input initial random particles and record the speed and position of each particle;
- Step 4. Calculate the fitness of each particle and record its own optimal position and the global optimal position of all particles;
- Step 5. Update the speed and position of the particles according to (18) and (19). Here, $v_i(k)$ and $x_i(k)$ represent the speed and position of particle i in the kth iteration, $rand_1$ and $rand_2$ represent the random number between 0 and 1, x^{gbest} represents the global optimal position of all particles, and x_i^{pbest} represents the historical optimal position of particle i;

$$v_i(k+1) = w \cdot v_i(k) + c_1 \cdot rand_1 \cdot [x_i^{pbest}(k) - x_i(k)] + c_2 \cdot rand_2 \cdot [x^{gbest}(k) - x_i(k)] \qquad (18)$$

$$x_i(k+1) = x_i(k) + v_i(k+1) \qquad (19)$$

- Step 6. According to (20) and (21), a quasi-opposite population is generated, which is incorporated into the initial population to form a mixed population. Here, x_i^m represents the value of the mth dimension decision variable in particle i, α_i^m and β_i^m represent the maximum and minimum values of x_i^m, and $\overline{x}_i^m$ and $\overline{X}_i^m$ represent the opposite and quasi-opposite values of x_i^m, respectively;

$$\overline{x}_i^m = \alpha_i^m + \beta_i^m - x_i^m \qquad (20)$$

$$\overline{X}_i^m = rand\left[\frac{\alpha_i^m + \beta_i^m}{2}, \overline{x}_i^m\right] \qquad (21)$$

- Step 7. Update the Pareto solution set X;
- Step 8. Determine whether the maximum number of iterations is reached. If yes, proceed to the next step. Otherwise, repeat Step 4–Step 7;
- Step 9. Output the optimal Pareto solution set.

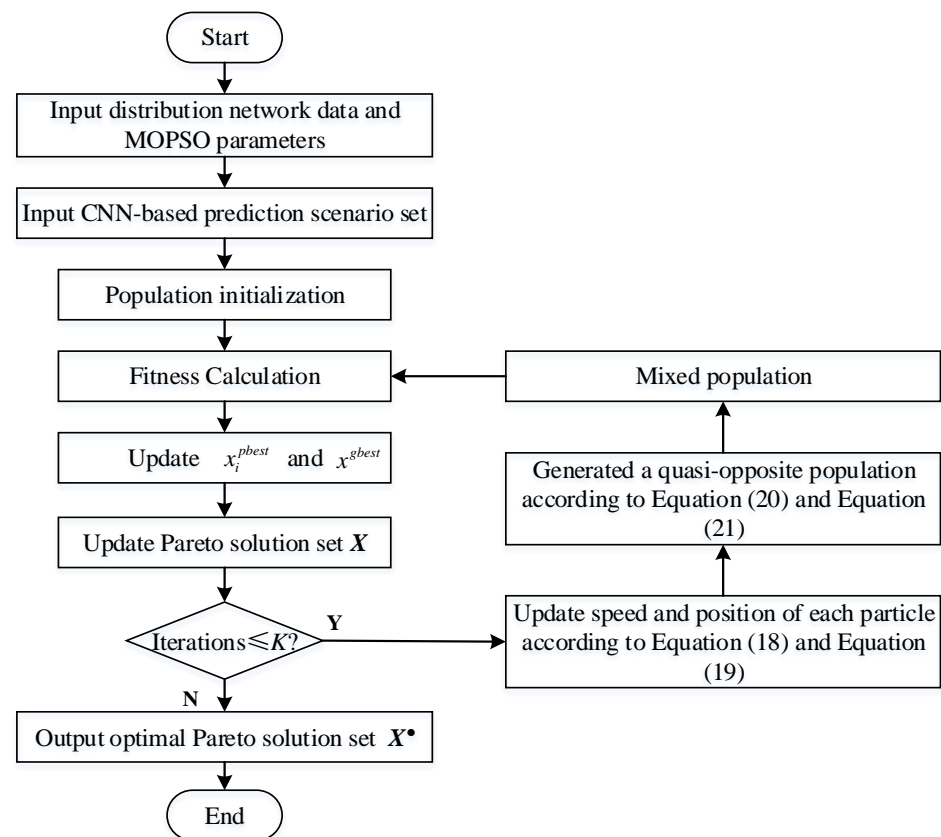The specific algorithm flow chart is shown in Figure 4.

Figure 4. Flow chart of the model solution based on the improved MOPSO algorithm.

5. Case Study

5.1. Parameter Settings

In this study, a standard IEEE-33 bus system is adopted to verify the effectiveness of the proposed optimal planning solution in the distribution network, as shown in Figure 5. The reference voltage of the distribution network system is 10 kV, the reference capacity is 8 MW, the total active load in the system is 4.125 MW, and the load access points are {13, 16, 19, 21, 27, 31}. The related data of PV and load used in this paper are from the NREL data set [25], and their characteristic profiles are shown in Figure 6.
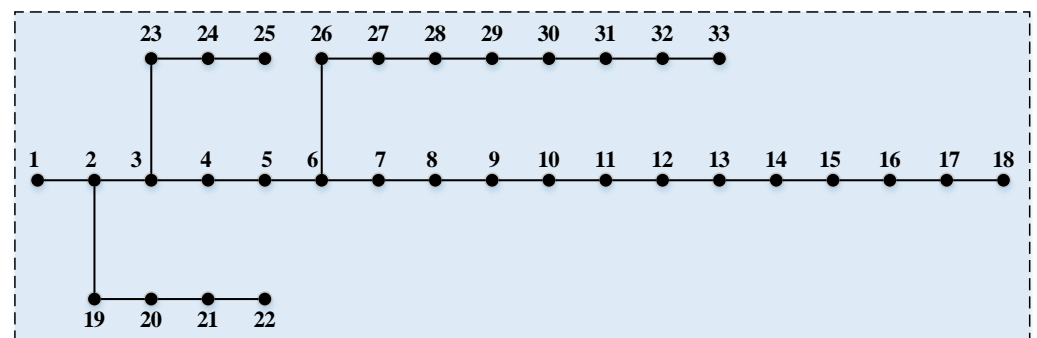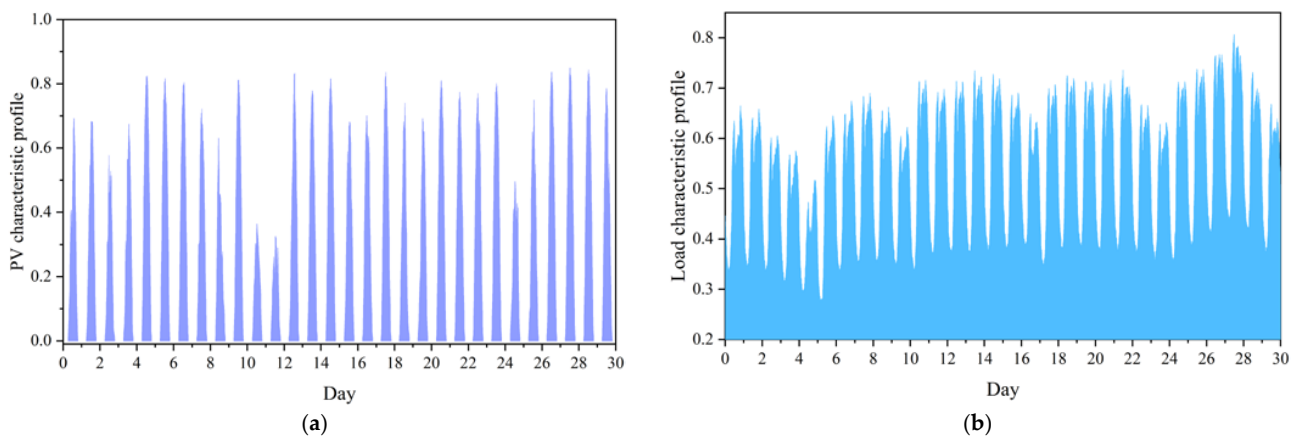

Figure 5. Typical IEEE-33 bus system.

Figure 6. The characteristic profiles of PV (**a**) and load (**b**) in 30 days.

The parameters of various equipment in the optimization model and the parameters of the improved PSO algorithm are shown in Table 1; the time-of-use price of electricity from the grid is shown in Table 2.

Table 1. Basic parameter settings in the proposed solution.

Parameter	Value
Investment cost of PV ($/kW)	4200
Investment cost of ESS ($/kWh)	2000
Investment cost of transmission line ($/km)	80000
Operation and Maintenance cost of PV ($/(kW·year))	800
Operation and Maintenance cost of ESS ($/(kWh·year))	620
SOC of ESS	0.1–0.9
Energy efficiency of ESS	0.88
Total planning years (year)	10
Discount rate	0.06
Carbon emission coefficient of thermal power generation ($kgCO_2$/kWh)	1.05
Carbon trading price ($/t)	60
Per-unit value of node voltage	0.82–1.16
Maximum transmission power of transmission line (kW)	600
Learning factors c_1 and c_2	1.58, 1.63
Weight coefficient w	0.9
Number of particles N	100
Iterations K	1000

Table 2. Time-of-use price of electricity from the grid.

	Time	Price ($/kWh)
Valley Period	0:00–8:00 23:00–24:00	0.28
Normal Period	8:00–10:00 15:00–18:00 21:00–23:00	0.55
Peak Period	10:00–15:00 18:00–21:00	0.84

For PV and load forecasting, this paper selects the data from January 2020 to December 2020. The first 25 days of each month are selected as the training sample and the remaining days of each month are selected as the test sample; the sampling interval is 10 min. The 144 power points in one day is reconstructed into a 12 × 12 matrix. The specific parameter settings of the CNN-based prediction model adopted in this paper are shown in Table 3. The convolutional kernel dimensions of the convolutional layers are 3 × 3 × 4 and 3 × 3 × 16, respectively. The activation function of the fully connected layer is *Re_lu*.

**Table 3.** The specific parameter settings of the CNN-based prediction model.

| Layer	Type	Dimension
1	Input	(12,12)
2	Convolution	(12,12,4)
3	Convolution	(12,12,16)
4	Flatten	(2304)
5	Fully connected	(144)
6	Output	(144)

The hardware environment in this paper is as follows: Intel (R) Core (TM) i5-3550; 8 GB RAM; and NVIDIA GeForce GTX 1060. The software environment is as follows: Matlab 2019a; and Matpower 6.0.

5.2. Forecasting Results of PV and Load

After training, the CNN model is used to predict the PV generation and load power on typical days in four different seasons, and the specific results are shown in Figures 7 and 8. It can be seen that the prediction model can effectively track the changes of PV and load, the prediction performance is ideal, and the needs of the subsequent planning model can be basically met. According to the calculation results, the maximum value of the mean absolute percentage error (MAPE) is 6.673% in PV forecasting and 5.421% in load forecasting.
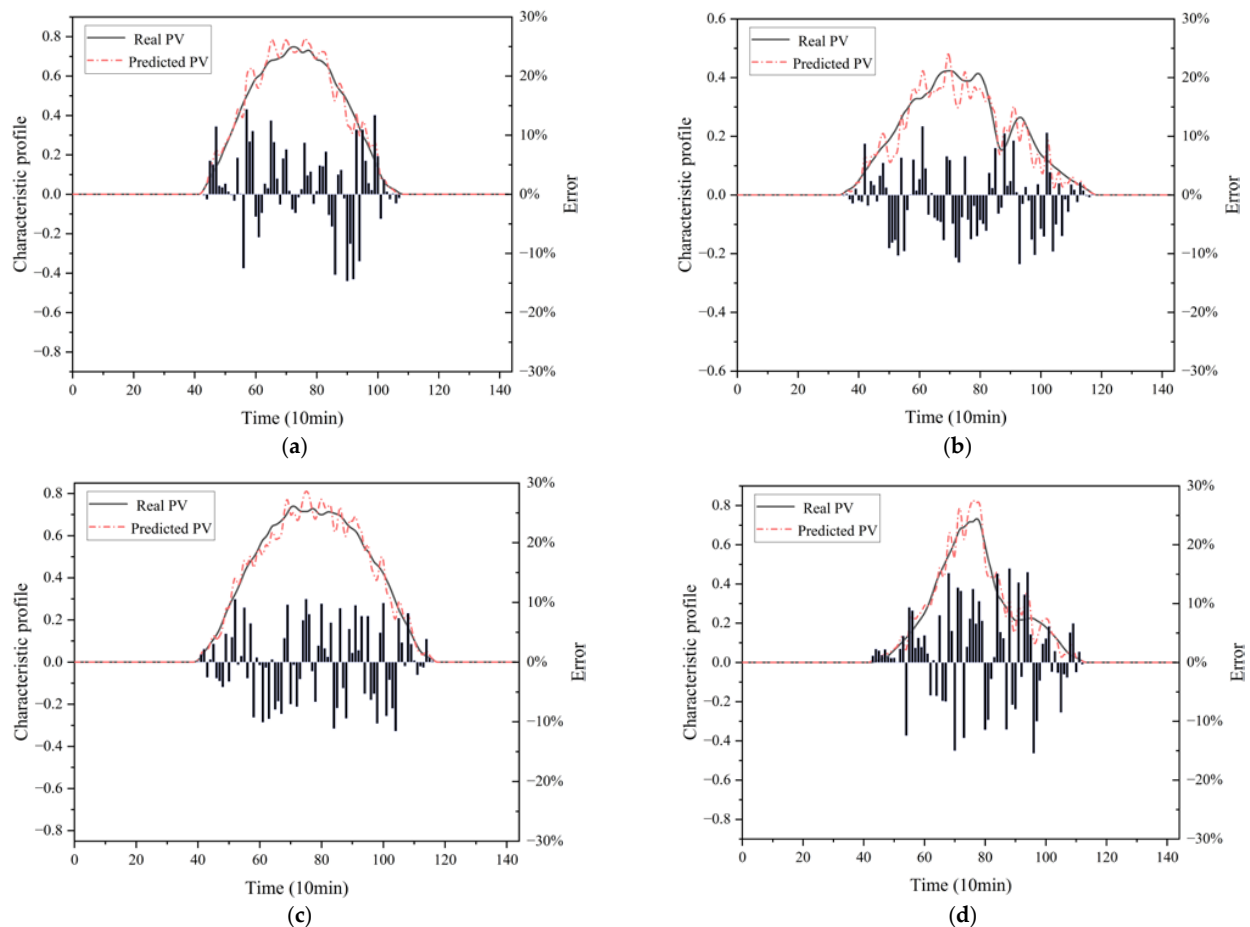
Figure 7. The prediction results and deviations of PV on four typical days. (**a**) Spring; (**b**) Summer; (**c**) Autumn; (**d**) Winter.
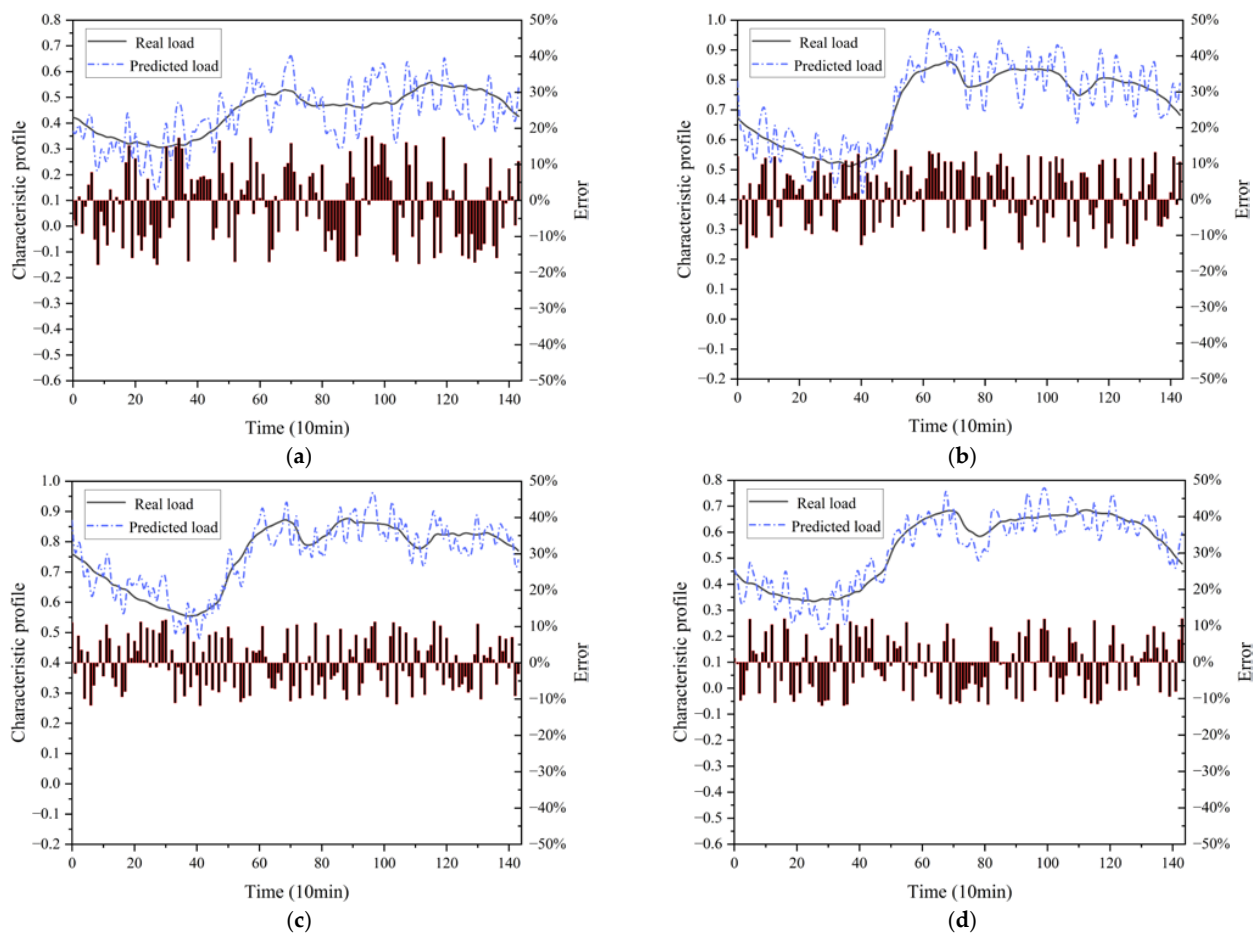
Figure 8. The prediction results and deviations of the load on four typical days. (**a**) Spring; (**b**) Summer; (**c**) Autumn; (**d**) Winter.

5.3. The Optimal Location and Capacity Configuration Results

Based on the scenario generation results of PV and load, the access location and configuration capacity of PV and ESS in the distribution network system are planned, and the improved MOPSO algorithm is used to optimize the model. Finally, the effectiveness of the proposed method is proved by comparing the following planning strategies:

- **Strategy I:** PV and ESS collaborative planning in the distribution network, without considering carbon emissions and multiple uncertainties (traditional configuration method);
- **Strategy II:** PV and ESS collaborative planning in the distribution network, in which multiple uncertainties are considered while carbon emissions are not;
- **Strategy III:** PV and ESS collaborative planning in the distribution network, in which carbon emissions and multiple uncertainties are considered (planning method proposed in this paper).

The optimization results and various indicators of the system under different planning strategies are shown in Tables 4 and 5, respectively.

Table 4. The optimal location and capacity configuration results of PV and load in DNs.

Device	Location			Capacity (MW, MWh)		
	I	II	III	I	II	III
PV	3	3	4	0.85	0.97	1.48
	6	8	10	0.86	1.04	1.75
	15	13	16	1.72	1.88	1.87
	30	20	20	1.34	1.53	0.92
		28	24	-	0.24	0.83
	-	-	29	-	-	0.16
Energy storage	8	6	4	1.27	1.32	1.45
	20	15	13	0.96	1.09	1.82
	-	28	31	-	0.42	0.66

Table 5. The various indicators in the model under different strategies.

Objectives	I	II	III
Investment cost (10^6 $)	24.49	29.43	37.30
Operation cost (10^6 $)	5.19	6.28	8.04
Electricity purchase cost (10^6 $)	24.83	20.07	13.19
Transmission line cost (10^6 $)	0.96	0.96	0.96
Total cost (10^6 $)	55.48	56.74	59.49
Carbon emission (t/CO_2)	3056.67	2776.03	2310.39
Reliability	1.622	1.936	2.563

Compared with strategy I, strategy II fully considers the uncertainties of PV and load in the distribution network, and a CNN-based scenario generation model is adopted to characterize their uncertainties; in strategy III, carbon emission constraints are added to the optimization model. It can be seen from Table 4 that the total configured capacities of PV and ESS are 4.77 MW and 2.23 MWh in strategy I, 5.66 MW and 32.83 MWh in strategy II, and 7.01 MW and 3.93 MWh in strategy III, respectively. The configured capacities in strategy I, II, and III are increasing, and it can be concluded that: (1) Compared with strategy I, the uncertainties of PV and load are fully considered in strategy II. In order to ensure the power supply reliability of the system, the configuration capacity of the PV generation equipment is increased, which results in the enhancement of the power supply stability and the improvement of the PV utilization rate. (2) Compared with strategy II, carbon emission constraints have been added to the optimization model in strategy III; thus, more PV generation and ESS equipment are installed to reduce the carbon emissions in the system.

Table 5 compares the economic indicators, carbon emissions, and power supply stability of the system under different optimization schemes. It can be seen that, when compared with Strategy I, the investment cost and operation cost in Strategy II increased by $4.94 M and $1.09 M, respectively, and the power purchase cost decreased by $4.76 M; the total cost of the system increased by 2.27%, but the reliability of the power supply is greatly improved, and the importance of uncertainty characterization is fully proved through this comparison. In addition, compared with Strategy II, the investment cost and operation cost in Strategy III increased by $7.87 M and $1.76 M, and the power purchase cost decreased by $6.88 M; the total cost of the system increased by only 4.85%, but the carbon emissions of the system decreased significantly (465.64 t CO_2); therefore, the impact of the carbon emission constraints on the DN planning is presented through this comparison. In conclusion, the optimal planning model for PV and ESS that accounts for the multiple uncertainties proposed in this paper can effectively reduce the carbon emissions of the system, improve the utilization rate of PV, and mitigate the impact caused by the massive connection of PV on the distribution network. The optimal location results for PV and ESS are shown in Figure 9.
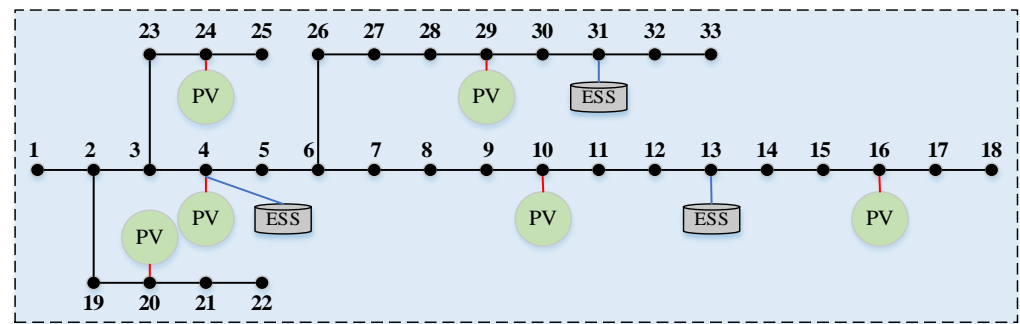
Figure 9. The optimal location results for PV and ESS.

6. Conclusions and Future Work

This paper proposes a novel optimal location and capacity configuration model for PV and ESS in a DN. Multiple uncertainties are considered and the following conclusions can be made: the CNN-based uncertainty characterization model can capture the probability characteristics of PV and load data effectively and fully characterize their uncertainties. Thus, the impact of the uncertainties of PV and load on the distribution network planning can be solved. Then, taking the minimum total economic cost of the system, the maximum carbon emission reduction, and the optimal power supply reliability as the objective functions, an optimal location and capacity configuration model for PV and ESS that considers multiple uncertainties in the DN is formulated. Finally, an improved MOPSO algorithm is used to solve the model, and the effectiveness of the proposed solution is proved through a comparative case study on the IEEE-33 bus system.

For future work, there still remain several crucial issues that are worthy of further exploration: the renewable source in the distribution network used in this paper only includes PV, and the energy storage is battery energy storage; however, in the actual distribution network, a single type of energy storage cannot fully meet the demand. Therefore, a variety of different types of DGs and energy storage equipment should be added to make the distribution network planning more comprehensive and reasonable.

References

1. Kourkoumpas, D.-S.; Benekos, G.; Nikolopoulos, N.; Karellas, S.; Grammelis, P.; Kakaras, E. A review of key environmental and energy performance indicators for the case of renewable energy systems when integrated with storage solutions. *Appl. Energy* **2018**, *231*, 380–398. [CrossRef]
2. Yang, Y.; Bremner, S.; Menictas, C.; Kay, M. Battery energy storage system size determination in renewable energy systems: A review. *Renew. Sustain. Energy Rev.* **2018**, *91*, 109–125. [CrossRef]
3. Liang, X. Emerging Power Quality Challenges due to Integration of Renewable Energy Sources. *IEEE Trans. Ind. Appl.* **2017**, *53*, 855–866. [CrossRef]
4. Ehsan, A.; Yang, Q. Optimal integration and planning of renewable distributed generation in the power distribution networks: A review of analytical techniques. *Appl. Energy* **2018**, *210*, 44–59. [CrossRef]
5. Kumar, M.; Soomro, A.M.; Uddin, W.; Kumar, L. Optimal Multi-Objective Placement and Sizing of Distributed Generation in Distribution System: A Comprehensive Review. *Energies* **2022**, *15*, 7850. [CrossRef]
6. Rynska, E. Review of PV Solar Energy Development 2011–2021 in Central European Countries. *Energies* **2022**, *15*, 8307. [CrossRef]
7. Zakaria, A.; Ismail, F.B.; Lipu, M.S.H.; Hannan, M.A. Uncertainty models for stochastic optimization in renewable energy applications. *Renew. Energy* **2020**, *145*, 1543–1571. [CrossRef]

8. Lin, P.; Peng, Z.; Lai, Y.; Cheng, S.; Chen, Z.; Wu, L. Short-term power prediction for photovoltaic power plants using a hybrid improved Kmeans-GRA-Elman model based on multivariate meteorological factors and historical power datasets. *Energy Convers. Manag.* **2018**, *177*, 704–717. [CrossRef]

9. Eseye, A.T.; Zhang, J.; Zheng, D. Short-term photovoltaic solar power forecasting using a hybrid Wavelet-PSO-SVM model based on SCADA and Meteorological information. *Renew. Energy* **2018**, *118*, 357–367. [CrossRef]

10. Yu, Y.; Wang, M.; Yan, F.; Yang, M.; Yang, J. Improved convolutional neural network-based quantile regression for regional photovoltaic generation probabilistic forecast. *IET Renew. Power Gener.* **2020**, *14*, 2712–2719. [CrossRef]

11. Dong, W.; Yang, Q.; Fang, X. Multi-Step Ahead Wind Power Generation Prediction Based on Hybrid Machine Learning Techniques. *Energies* **2018**, *11*, 1975. [CrossRef]

12. Hernández, L.; Baladrón, C.; Aguiar, J.M.; Calavia, L.; Carro, B.; Sánchez-Esguevillas, A.; Pérez, F.; Fernández, A.; Lloret, J. Artificial Neural Network for Short-Term Load Forecasting in Distribution Systems. *Energies* **2014**, *7*, 1576–1598. [CrossRef]

13. Zhang, F.; Deb, C.; Lee, S.E.; Yang, J.; Shah, K.W. Time series forecasting for building energy consumption using weighted Support Vector Regression with differential evolution optimization technique. *Energy Build.* **2016**, *126*, 94–103. [CrossRef]

14. Lin, W.M.; Tu, C.S.; Yang, R.F.; Tsai, M. Particle swarm optimisation aided least-square support vector machine for load forecast with spikes. *IET Gener. Transm. Distrib.* **2016**, *10*, 1145–1153. [CrossRef]

15. Kong, W.; Dong, Z.Y.; Hill, D.J.; Luo, F.; Xu, Y. Short-Term Residential Load Forecasting Based on Resident Behaviour Learning. *IEEE Trans. Power Syst.* **2018**, *33*, 1087–1088. [CrossRef]

16. Jiang, Y.; Kang, L.; Liu, Y. Optimal configuration of battery energy storage system with multiple types of batteries based on supply-demand characteristics. *Energy* **2020**, *206*, 118093. [CrossRef]

17. Bragatto, T.; Carere, F.; Cresta, M.; Gatta, F.; Geri, A.; Lanza, V.; Maccioni, M.; Paulucci, M. Location and sizing of hydrogen based systems in distribution network for renewable energy integration. *Electr. Power Syst. Res.* **2022**, *205*, 107741. [CrossRef]

18. Yi, J.; Cherkaoui, R.; Paolone, M.; Shchetinin, D.; Knezovic, K. Expansion planning of active distribution networks achieving their dispatchability via energy storage systems. *Appl. Energy* **2022**, *326*, 119942. [CrossRef]

19. Dash, S.K.; Mishra, S.; Abdelaziz, A.Y.; Hong, J.; Geem, Z.W. Optimal Planning of Multi-type DGs and D-STATCOMs in Power Distribution Network Using an Efficient Parameter Free Metaheuristic Algorithm. *Energies* **2022**, *15*, 3433. [CrossRef]

20. Barukčić, M.; Varga, T.; Benšić, T.; Jerković Štil, V. Optimal Allocation of Renewable Energy Sources and Battery Storage Systems Considering Energy Management System Optimization Based on Fuzzy Inference. *Energies* **2022**, *15*, 6884. [CrossRef]

21. El-Ela, A.A.A.; El-Sehiemy, R.A.; Abbas, A.S. Optimal Placement and Sizing of Distributed Generation and Capacitor Banks in Distribution Systems Using Water Cycle Algorithm. *IEEE Syst. J.* **2018**, *12*, 3629–3636. [CrossRef]

22. Kashyap, M.; Kansal, S.; Verma, R. Sizing and Allocation of DGs in A Passive Distribution Network Under Various Loading Scenarios. *Electr. Power Syst. Res.* **2022**, *209*, 108046. [CrossRef]

23. Ghaffari, A.; Askarzadeh, A.; Fadaeinedjad, R. Optimal allocation of energy storage systems, wind turbines and photovoltaic systems in distribution network considering flicker mitigation. *Appl. Energy* **2022**, *319*, 119253. [CrossRef]

24. Agga, A.; Abbou, A.; Labbadi, M.; El Houm, Y. Convolutional Neural Network (CNN) Extended Architectures for Photovoltaic Power Production Forecasting. In Proceedings of the 2021 9th International Conference on Smart Grid and Clean Energy Technologies (ICSGCE), Sarawak, Malaysia, 15–17 October 2021; pp. 104–108.

25. Draxl, C.; Clifton, A.; Hodge, B.-M.; McCaa, J. The wind integration national dataset (wind) toolkit. *Appl. Energy* **2015**, *151*, 355–366. [CrossRef]